Single-cell RNA sequencing analysis and transgenic mouse models reveal differential effects of flash vs. standard proton radiotherapy on gastrointestinal tissues and tumors

Ioannis I. Verginadis[1], Clara Morral Martinez[1], Priyanka Chowdhury[1], Giorgos Skoufos[2,3], Michele M. Kim[1], Anastasia Velalopoulou[1], Denisa Goia[1], Leo Luo[1], Caitlin J. Foley[1], Zachary J. Reitman[4], Andrea R. Daniel[4], Eric Diffenderfer[1], Lei Dong[1], James Metz[1], David G. Kirsch[4], Andy Minn[5] and Constantinos Koumenis[1]

[1]Department of Radiation Oncology, Perelman University School of Medicine, University of Pennsylvania, Philadelphia, PA, USA

[2]Department of Electrical and Computer Engineering, University of Thessaly, Volos, Greece

[3]Hellenic Pasteur Institute, Athens, Greece

[4]Department of Radiation Oncology, Duke University Medical Center, Durham, NC, USA

[5]Department of Radiation Oncology, Perelman University School of Medicine, University of Pennsylvania, Philadelphia, PA; Abramson Family Cancer Research Institute, Perelman School of Medicine, University of Pennsylvania, Philadelphia; Parker Institute for Cancer Immunotherapy at University of Pennsylvania, Philadelphia, PA; Mark Foundation Center for Immunotherapy, Immune Signaling, and Radiation, University of Pennsylvania, Philadelphia, PA, USA

Recent studies suggest that ultrahigh-dose-rate, "FLASH," radiation therapy (RT) decreases normal tissue damage while maintaining tumor response compared with conventional dose rate RT. Our group has designed and tested the first system to accurately deliver dosimetrically identical FLASH Proton RT (F-PRT; 60-110 Gy/sec) or Standard Proton RT (S-PRT; 0.5-1 Gy/sec) using double-scattered protons. Our purpose is to identify if F-PRT is superior to S-PRT in protecting normal tissues, while equipotent in controlling tumor growth. We previously demonstrated that compared to S-PRT, F-PRT significantly decreases overall mortality from late epithelial gastrointestinal (GI) fibrosis (p<0.005) in mouse models following 14 (males) and 15 Gy (females) whole-abdomen and 18 Gy focal intestinal RT, whereas tumor growth inhibition is essentially indistinguishable between the two modalities. We also found that F-PRT-treated mice displayed a significantly higher percentage of regenerated crypts (EdU incorporation) in comparison to the S-PRT (p<0.01). To better understand the differential responses of the normal intestine between the two treatment modalities, we performed single-cell RNA sequencing on 14 Gy F-PRT and S-PRT-treated intestines at 2, 10, and 20 days post-RT. Analysis revealed enrichment of stem/progenitor epithelial cell populations with increased proliferative signatures and expression of genes related to the interferon-alpha signature in epithelial and immune cells post F-PRT treatment compared to the S-PRT. Immunofluorescence staining of F-PRT and S-PRT treated intestinal tissues confirmed a) the higher proliferation rate of epithelial cells observed in F-PRT-treated mice, b) significantly higher number of infiltrated immune cells in F-PRT- compared to the S-PRT-treated mice and c) higher expression of interferon signaling in immune cells in F-PRT treated mice. Collectively, our preliminary findings suggest that F-PRT may enhance a regenerative or facultative stem cell program that is associated with greater and more persistent IFN Type I signaling. Moreover, using a model of epithelial-specific knockout of p53 (Villin-Cre;p53), we found that mice treated with 13 Gy S-PRT quickly succumb to acute radiation GI syndrome, while F-PRT treated mice had significantly improved survival (median survival: 8.5 days for S-PRT vs 164 days for F-PRT; p<0.05). This suggests that F-PRT may preserve a higher proportion of progenitor epithelial cells with enhanced regeneration potential. Understanding the cellular and molecular basis for the effects of F-PRT provides a framework for clinical application of this novel modality with the potential to improve the therapeutic outcome and quality of life of cancer patients.

A transcriptomic atlas of the mouse skin irradiated with FLASH proton radiation

Anastasia Velalopoulou, Giorgos Skoufos, Michele Kim, Ioannis I. Verginadis, Artemis G. Hatzigeorgiou, Lei Dong, James Metz, Costantinos Koumenis, Keith Cengel, Amit Maity, Theresa M. Busch

ABSTRACT

Purpose: To investigate the transcriptomic changes induced by FLASH proton radiotherapy (F-PRT) that could be responsible for the protection of normal epithelial tissues by radiation-induced toxicities as have been previously shown by us and others. **Methods:** C57BL/6J mice received 30 Gy of F-PRT or S-PRT to the hind leg at respective dose rates of 69-124 Gy/sec or 0.39–0.65 Gy/sec. RNA sequencing was performed using full-thickness leg skin at 5 days after radiation revealing major pathways regulated by F-PRT and S-PRT. In an endeavor to identify the full repertoire of cells and gene expression profiles that are involved in the sparing effects of FLASH PRT, we expanded our studies to include single-cell RNA sequencing (sc-RNA seq) and examined additional time points such as Day 2 and Day 10 after radiation. Single-cell transcriptome libraries were generated on a 10X Genomics Chromium system. Datasets were acquired from cell samples derived and sequenced from pooled skin samples of three mice per group. Skin from the sequenced mice was also embedded for spatial analysis of gene expression. **Results**: RNA sequencing revealed that F-PRT uniquely upregulates almost four times more genes compared to S-PRT (F-PRT-uniquely upregulated 489 genes vs S-PRT-uniquely upregulated 129 genes). Also, F-PRT uniquely downregulated 178 genes, compared to the 125 genes uniquely downregulated by S-PRT. GO analysis demonstrates that the keratinization and apoptosis pathways are uniquely upregulated by S-PRT, whereas F-PRT uniquely upregulates genes involved in vascular development pathway. During submission of the abstract, analysis of sc-RNA seq samples was pending**. Conclusion**: Our comprehensive studies inform on the transcriptomic profiling of skin cell populations that are affected by F-PRT vs S-PRT; this insight will further spur discoveries on the biology of FLASH radiotherapy effects.

Evaluation of Therapeutic Response to Dendritic Cell Vaccine Immunotherapy in Recurrent Glioblastomas using Multiparametric MRI

Sanjeev Chawla, PhD, DABMP

Department of Radiology, Perelman School of Medicine at the University of Pennsylvania, Philadelphia, PA

Background and Purpose: Glioblastoma (GBM) is an aggressive tumor, resistant to conventional treatment. Currently, immunotherapy is being used as an alternative treatment modality for recurrent GBMs in clinical trials. Immunotherapeutic approaches, such as dendritic cell (DC) vaccine, harness patient's immune response to eliminate tumor cells, and in turn produce profound inflammation at the tumor bed, often referred to as treatment-induced pseudoprogression (PsP). Standard MR imaging is not adequate for treatment response. Thus, there is an urgent need for the development of effective and alternative neuroimaging techniques for accurate response assessment. The purpose of present study was to investigate the potential of multiparametric MRI-based predictive model in the assessment of treatment response in recurrent GBM patients treated with DC vaccine.

Methods: Eighteen patients with recurrent GBM treated with DC vaccine (mean dose = 0.25 mL) who had initially undergone surgery followed by standard chemoradiation therapy, were included. All patients underwent anatomical imaging, diffusion tensor imaging (DTI), and dynamic susceptibility contrast (DSC)-perfusion imaging on a 3T MR system. When tumor specimen was available from repeat surgery, pathology was used to identify true progression (TP) (>25% malignant features; n=12) or PsP (<25%malignant features; n=1). In the case of non-availability of tumor specimens, >2 consecutive follow-up MRIs using mRANO criteria were assessed to determine TP (n=2) or PsP (n=3). The multiparametric model consisted of DTI derived fractional anisotropy (FA), linear anisotropy (CL), and DSC derived maximum relative cerebral blood volume (rCBV) from contrast-enhancing regions in differentiating TP from PsP. This model was used to compute the progression probabilities (PP) at the time point when TP was suspected on follow-up MRIs and repeat surgery was being contemplated. Thus, the most recent multiparametric MRI preceding re-resection/biopsy was used to calculate PP values which were then correlated with subsequent histopathologic findings. Lesions were considered TP if PP was ≥ 50% and PsP if PP was ≤ 50%. Based upon PP values, number of cases correctly classified as TP/PsP were determined. Pearson's test was performed to correlate findings of our predictive model with those of pathology and mRANO criteria. Kaplan-Meier analyses were performed using multiple independent variables.

Results: Representative anatomical images, DTI derived parametric maps, and CBV map are shown in **figure 1**. Our predictive model had overall concordance rate of 72.2% with the final diagnosis as determined by histopathology/mRANO criteria (9/14 TP and 4/4 PsP). While characterizing each lesion as TP or PsP, a significant correlation was observed between PP values and histopathology/mRANO criteria (r = 0.54; p = 0.02). PP values were higher in TP than in PsP cases (median= 72% vs. 19%). As shown in **figure 2**, Kaplan-Meier survival analyses revealed that PsP patients had significantly prolonged survival outcomes than TP/mixed tumor patients when patients were classified by histopathology/mRANO (37.3 ± 9.5 vs. 19.2 ± 1.7months, log-rank p=0.03, and multiparametric MRI derived predictive model (27.07± 5.5 vs. 19.4 ± 1.06months, log-rank p=0.02). Additionally, trends in longer overall survivals were observed from lower Ki-67, MGMT methylated and EGFRvIII negative patients compared to their counterparts.

Conclusion: Our findings indicate that multiparametric MRI may be helpful in assessing response to DC vaccine in recurrent GBM patients. However, this promising finding warrants further validation in future, larger clinical trials.
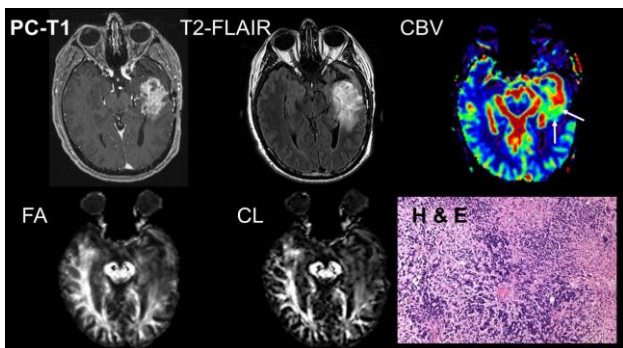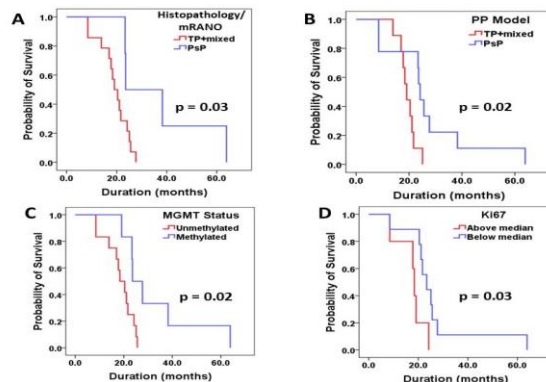

Fig. 1

Fig. 2

Improving the efficiency of small animal 3D printed compensator IMRT with total variation regularization

Xinmin Liu,   Khayrullo Shoniyozov,   Rodney D. Wiersma

Purpose: There is growing interest in the use of modern 3D printing technology to implement intensity-modulated radiation therapy (IMRT) on the preclinical scale that is analogous to clinical IMRT. However, current 3D-printed IMRT methods suffer from complex modulation patterns leading to long delivery times, excess filament usage, and less accurate compensator fabrication. In this work, we have developed a total variation regularization (TVR) approach to address these issues.

Methods: TVR-IMRT was used to optimize the beamlet intensity map, which was then converted to a thickness of the corresponding compensator attenuation region in copper-doped polylactic acid (PLA) filament. Both IMRT and TVR-IMRT were used to generat mice heart and lung plans. The total compensator thickness, total variation (TV) of compensator beamlet thicknesses, TV of beamlet intensities, and exposure time were compared. The individual field doses and composite dose were delivered to film for one plan and gamma analysis was performed.

Results: In total, 12 mice heart and lung plans were generated for both IMRT and TVR-IMRT cases. It was found that TVR-IMRT reduced the TV of compensator beamlet thicknesses and beamlet intensities by $54 \pm 4\%$ and $50 \pm 3\%$ on average when compared to standard 3D printed compensator IMRT. On average, the total mass of compensator material consumed and radiation beam-on time were reduced by $45 \pm 6\%$ and $24 \pm 4\%$, respectively, while dose metrics remained comparable. Heart plan compensators were printed and delivered to film and subsequent gamma analysis performed for each of the single fields as well as the composite dose. For the composite delivery, a passing rate of 89.1% for IMRT and 95.4% for TVR-IMRT was achieved for a 3%/0.3mm criterion.

Conclusions: TVR can be applied to small animal IMRT beamlet intensities in order to produce fluence maps and subsequent 3D-printed compensator patterns with significantly less complexity while still maintaining similar dose conformity to traditional IMRT. This can simplify/accelerate the 3D printing process, reduce the amount of filament required, and reduce overall beam-on time.
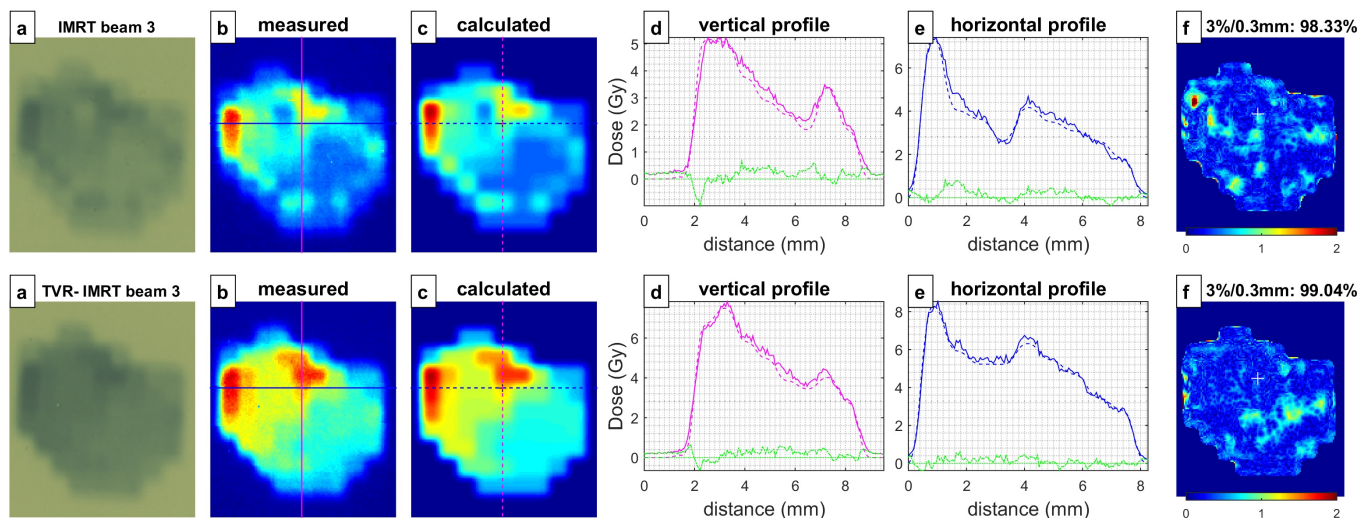
Figure 1: Gamma analysis of single field dose delivery for a lung plan (top: IMRT, bottom: TVR-IMRT)

ChoKα-targeted NIR fluorophore for optical surgical navigation in canine patients with spontaneous lung cancer

Sofya Osharovich[1,2], Michael Hart[1,2], Stefan Harmsen[1], Anatoliy Popov[1],
Sunil Singhal[3], Jennifer Huck[4], David Holt[4], Jim Delikatny[1,2]
Department of Radiology[1], Pharmacology Graduate Group[2], Department of Surgery[3], School of
Veterinary Medicine[4,], University of Pennsylvania

Introduction: Choline Kinase α (ChoKα) is an established cancer biomarker associated with an aggressive phenotype, high histological tumor grade, and poor clinical outcome in many human cancers. ChoKα is overexpressed in 60% of human lung tumors[1-3]. ChoKα catalyzes the phosphorylation of choline to generate phosphocholine, a precursor of the cell membrane phospholipid, phosphatidylcholine (PtdCho)[4]. A novel near-infrared (NIR) fluorescent ChoKα inhibitor, JAS239 (λ_{ex}: 745 nm, λ_{em}: 775 nm), has been developed in our lab [5]. JAS239 binds to the active site of ChoKα, competitively inhibiting phosphocholine production, and thus can be used to target ChoKα-overexpressing tumors for optical surgical navigation. Here, we report our results from a clinical trial in canine patients with spontaneous lung adenocarcinomas.

Methods: Canine patients with operable lung adenocarcinomas were recruited into the clinical trial. Patients (n=7) received 0.25, 0.5, or 1 mg/kg JAS239 24 hours prior to intraoperative imaging to determine the optimal dose. The VisionSense Imaging System was used to image the lung tumors *in situ* and *ex vivo* as well as involved lymph nodes. After tumor resection, the tumor was imaged on the back bench and sections of the tumor were cut and imaged. Cut pieces of the tumors were imaged on the LI-COR PEARL and submitted to the University of Pennsylvania School of Veterinary Medicine Comparative Pathology Core (CPC) for H&E and ChoKα immunohistochemistry (IHC).

Results: Intraoperative tumor imaging showed clear margin delineation with tumor to background ratios (TBR) of 2 (0.25 mg/kg), 6 (0.5 mg/kg), and 4 (1 mg/kg). IHC showed heterogeneous ChoKα expression, similar to humans.

Discussion and Conclusions: The purpose of these preliminary clinical cases is to establish the optimal dosing and timing for imaging JAS239 fluorescence in canine lung tumors. Patients receiving 0.5 mg/kg JAS239 yielded the highest TBR values due to the low background signal in normal lung tissue compared to the tumor signal. We are continuing our clinical trial to determining the efficacy of JAS239 for detecting tumor margins, metastases from other cancers, involved lymph nodes, and ChoKα levels. The ultimate goal of this study is translation of JAS239 for optical surgical navigation in human lung tumor patients.

References:
1. Cuadrado, A., *et. al.* "Phosphorylcholine: a novel second messenger essential for mitogenic activity of growth factors." *Oncogene* 8.11 (1993): 2959-2968. PMID: 8414498.
2. Molina, A., *et. al.* "Expression of Choline Kinase Alpha to Predict Outcome in Patients with Early-stage Non-small-cell Lung Cancer: A Retrospective Study." *The Lancet Oncology* 8.10 (2007): 889-97. PMID: 17851129.
3. Molina, A., *et. al.* "Overexpression of Choline Kinase Is a Frequent Feature in Human Tumor-derived Cell Lines and in Lung, Prostate, and Colorectal Human Cancers." *Biochemical and Biophysical Research Communications* 296.3 (2002): 580-83. PMID: 12176020.
4. Arlauckas, Sean P., et al. "Choline Kinase Alpha—Putting the ChoK-Hold on Tumor Metabolism." *Progress in Lipid Research*, vol. 63, 2016, pp. 28–40., PMID: 27073147.
5. Arlauckas, Sean P., et al. "Direct Inhibition of Choline Kinase by a Near-Infrared Fluorescent Carbocyanine." *Molecular Cancer Therapeutics*, vol. 13, no. 9, 2014, pp. 2149–2158., PMID: 25028471.

Real-time spectral CT thermometry via physical density for image-guided tumor ablation

Leening P. Liu[1,2], Matthew Hung[2], Michael C. Soulen[2], Nadav Shapira[2], Peter B. Noël[2]
[1]Department of Bioengineering, University of Pennsylvania, Philadelphia, USA,
[2]Department of Radiology, University of Pennsylvania, Philadelphia, USA

Hepatocellular carcinoma, the fastest rising cause of cancer-related deaths, is commonly treated with percutaneous ablative therapies where tumor cells are destroyed once tissue temperatures reach a lethal threshold. However, high progression and recurrence rates post ablation suggest the need for intraprocedural temperature monitoring to ensure the lethal threshold (>60 °C) is reached and a sufficient safety margin is obtained. Based on our preliminary developments, we can generate physical density maps using spectral CT data. These spectral physical density quantifications enable thermometry by taking advantage of the thermal volumetric expansion equation that relates the change in temperature to physical density changes. To validate the physical density model, an ex vivo bovine muscle was weighed and scanned on a clinical spectral CT scanner with different scanning parameter combinations (collimation, dose, helical/axial scans). Calculated mass from physical density maps and volume demonstrated high accuracy with a maximum percent error of 0.34% (<1.1 grams for a 345 gram sample) and minimal effects of scanning parameters. After validating the accuracy of the physical density maps, the muscle was subjected to heating and cooling while scanning to evaluate the relationship between physical density and temperature. Spectral CT results were continuously generated to calculate physical density maps at different temperatures. A linear relationship between change in temperature and change in physical density was established with strong correlation (R = 0.9781). The reflection of thermal volumetric expansion in physical density quantifications indicate its potential utility for providing real-time temperature feedback to image-guided cancer therapy during ablative procedures for not only hepatocellular carcinoma, but also other types of malignancies.
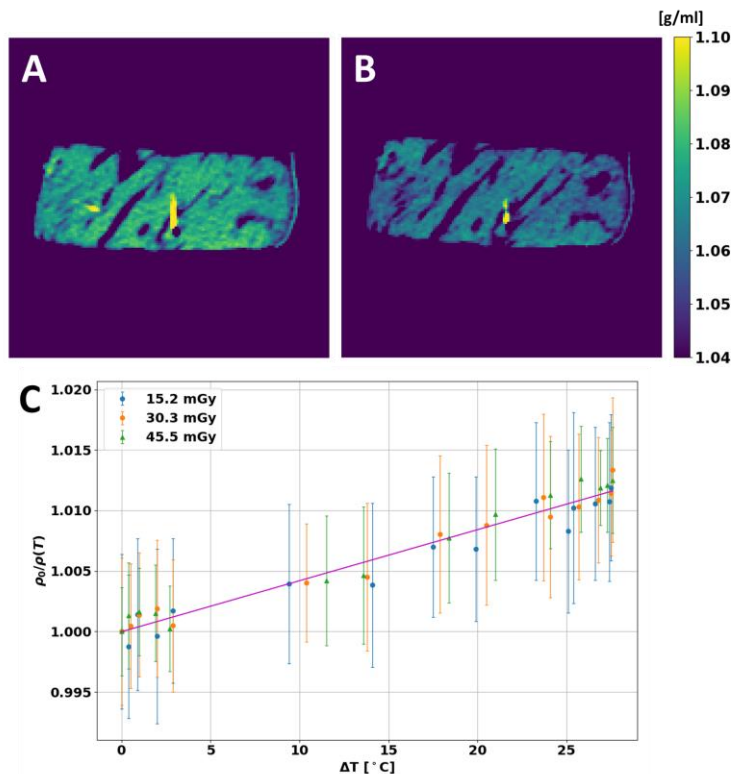
Figure. Changes in physical density during heating and cooling of *ex vivo* bovine muscle. Physical density maps of ex vivo bovine muscle in water (ρ = 1 g/cm³) at 22 °C (A) and 45.5 °C (B) demonstrated decreased physical density with increased temperatures. (C) The physical density ratio and temperature changes illustrated a linear relationship that reflects thermal volumetric expansion.

Dose verification with Cherenkov imaging for TSET patients

W Zhong, T C Zhu, T Miao, Y Zhu, C Sun, A Dimofte, L Dong, A Maity, I Paydar, J Plastaras

Purpose: Cherenkov imaging is being applied to TSET as a non-invasive and real-time remote monitoring technique. It can be used to verify delivered dose on patients' skin surface of whole body, instead of several locations from *in-vivo* OSLD measurements. To obtain dose distributions from Cherenkov images, determination of 2D Cherenkov-to-dose conversion factors is necessary. Monte Carlo (MC) simulations with realistic patient geometries verify both dose and Cherenkov light distributions on patient skin and provides a method to determine 2D Cherenkov-to-dose conversion factors.

Methods: A large PVC board (1.2 m x 2.4 m) positioned at TSET clinical setting was used to study the relationship between dose and Cherenkov intensity on the flat 2-D plane. MC simulations of the PVC board quantitatively verified the deviation of Cherenkov light from dose distributions along vertical directions in dual-field beams, which was observed in measured dose with in-vivo OSLD and Cherenkov images with CCD cameras. MC study also helped to identify that the major source of the deviation is the spoiler plate, which has been confirmed by the consistent distributions of measured dose and Cherenkov images after removing the spoiler plate in clinic. To obtain the realistic Cherenkov-to-dose relationship for each TSET patient, spoiler plate is kept in position in MC simulations with realistic patient geometries in the format of CT DICOM files. The realistic patient geometries were converted from a Finite Element Model of patient body after deformable registration with specific patient geometry of real-time 3D scan during treatment. The 2D Cherenkov-to-dose conversion factors for each patient are determined by the ratios of the normalized MC Cherenkov intensity distributions and the normalized MC surface dose distributions, both are normalized to the prescribed umbilicus location.

Results: On the PVC board, the 2D conversion factors along vertical directions were found to be less than 15%, and the major cause of the deviation of Cherenkov light from dose distributions was the spoiler plate. For the 18 patients evaluated, the conversion factors obtained by ratios of *in-vivo* OSLDs and Cherenkov images at the locations of chest, right hand, perineum, right shin, and vertex were found to be 1.07 ± 0.07, 1.10 ± 0.09, 1.32 ± 0.02, 1.8 ± 0.3, 1.4 ± 0.3 respectively. The 2D conversion factors determined from MC simulations of five patients up to now are consistent with the ratios at measured locations.

Conclusion: Monte Carlo simulations in patient specific geometries provide a practical way to determine the 2D Cherenkov-to-Dose conversion factors that agree with *in-vivo* OSLD measurements. With the 2D conversion factors of each posture, the delivered dose distribution of each posture and delivered cumulative dose of a full TSET treatment cycle for each patient can be obtained from their Cherenkov images which are measured in real-time during treatment.

Surgery-induced immunosuppression limits photodynamic therapy efficacy for mesothelioma

Gwendolyn M. Cramer, Richard W. Davis IV, Astero Klampatsa, Shirron Carter, Joann Miller, Keith A. Cengel, Theresa M. Busch

Lung-sparing radical pleurectomy with intraoperative photodynamic therapy (PDT) promisingly extends survival for patients with malignant pleural mesothelioma (MPM). Nevertheless, most patients treated with this multimodal approach go on to develop local tumor recurrence, so it is crucial to determine potential mechanisms that prompt treatment failure and develop mitigation strategies. Surgery is known to induce inflammation, and we have seen in our preclinical models of murine MPM given simulated surgery (tumor injury without cytoreduction) followed by Photofrin-PDT that the surgical procedure diminishes the curative potential of PDT. To further explore the mechanisms by which surgically induced inflammation might diminish PDT efficacy, we have used these murine MPM tumor injury/PDT models to determine key leukocyte players in the development of local tumor response and establishment of long-term systemic tumor control. Using flow cytometry-based immunophenotyping and functional studies focusing on myeloid-derived suppressor cells and T cells, we have found distinct patterns of innate and adaptive inflammatory cells in tumors, tumor draining lymph nodes, and spleens of MPM tumor bearing animals. Overall, these studies suggest that surgically mediated modulation of immune cell trafficking and functionality prior to PDT leads to a systemic suppression of PDT-induced anti-tumor immune response. Targeted inhibition of these molecular or cellular signals of surgically induced inflammation may reestablish PDT efficacy in the intraoperative setting.

Development of a phospholipase A2 activatable fluorophore for human and canine lung cancer imaging

Michael C. Hart[1], Drew Ramos[1], Andrea E. Rodriguez[1], Sofya A. Osharovich[1], Stefan Harmsen[1], David E. Holt[2], Anatoliy V. Popov[1], Sunil Singhal[3], Edward J. Delikatny[1]

[1]Department of Radiology, Perelman School of Medicine, University of Pennsylvania, Philadelphia, PA, USA; [2]Department of Clinical Studies, School of Veterinary Medicine, University of Pennsylvania, Philadelphia, PA, USA; [3]Division of Thoracic Surgery, Department of Surgery, University of Pennsylvania, Philadelphia, PA, USA

Introduction: Lung cancer is the leading cause of cancer-related death in the United States.[1] Approximately 85% of lung cancers are non-small cell lung cancers (NSCLC) which are primarily treated by surgical resection of the disease. NSCLC resections rely on tissue palpation and visual inspection to identify margins. This nonspecific identification leads to roughly 40% of NSCLC patients experiencing disease recurrence.[2,3] Thus, targeted imaging agents for the intraoperative detection of NSCLC would improve rates of curative resections. Cytosolic phospholipase A2 (cPLA2) is overexpressed and hyperactive in NSCLC. Our lab previously developed a PLA2 activatable fluorophore for triple-negative breast cancer (TNBC) imaging, DDAO-arachidonate (DDAO-A).[4-6] Due to the high cPLA2 expression and mortality rate associated with NSCLC, we hypothesized that DDAO-arachidonate would be preferentially activated in human and canine lung cancer tissues when compared to normal lung tissues making it a promising agent for real-time guidance of NSCLC surgical resections.

Methods: Human (n=10) and canine (n=3) normal lung and lung tumor tissues were obtained from patients at the Hospital of the University of Pennsylvania and the School of Veterinary Medicine. Tissues were treated topically with DDAO-A, and fluorescence was measured after 15 min. Five KLN 205 tumor-bearing DBA/2 mice, a NSCLC model, were treated intratumorally with DDAO-A, a negative control probe called DDAO-palmitate (DDAO-P), or with DDAO-P chased by DDAO-A to rescue fluorescence activation. Tumors and flank muscle tissues were excised from all mice and imaged for *ex vivo* fluorescence.

Results: In 8 out of 10 human and in all canine specimens, tissues exhibited fluorescent tumor-to-normal ratios (TNRs) of 2:1 or higher demonstrating that DDAO-A is preferentially activated in lung tumor tissues. Mice treated with the negative control probe, DDAO-P, exhibited insignificant increases in tumor fluorescence. DDAO-A chase treatments and initial intratumoral injections resulted in significant increases in the signal-to-noise ratios (SNR) showing strong activation of DDAO-A in tumors with SNRs up to 9.47:1.

Conclusions: DDAO-A is preferentially activated by lung tumor tissues in mouse models and in human and canine specimens. TNRs of 2:1 and higher demonstrated tumor selectivity making the probe a promising candidate for the real-time guidance of surgical resections.

1. Cancer Facts & Figures. American Cancer Society. 2022. https://www.cancer.org/research/cancer-facts-statistics/all-cancer-facts-figures/cancer-facts-figures-2022.html
2. Kelsey CR, Clough RW, Marks LB. Local recurrence following initial resection of NSCLC: salvage is possible with radiation therapy. *Cancer J*. Jul-Aug 2006;12(4):283-8. doi:10.1097/00130404-200607000-00006
3. Uramoto H, Tanaka F. Recurrence after surgery in patients with NSCLC. *Transl Lung Cancer Res*. Aug 2014;3(4):242-9. doi:10.3978/j.issn.2218-6751.2013.12.05
4. Chiorazzo MG, Bloch NB, Popov AV, Delikatny EJ. Synthesis and Evaluation of Cytosolic Phospholipase A(2) Activatable Fluorophores for Cancer Imaging. *Bioconjug Chem*. Dec 16 2015;26(12):2360-70. doi:10.1021/acs.bioconjchem.5b00417
5. Chiorazzo MG, Tunset HM, Popov AV, Johansen B, Moestue S, Delikatny EJ. Detection and Differentiation of Breast Cancer Sub-Types using a cPLA2alpha Activatable Fluorophore. *Sci Rep*. Apr 16 2019;9(1):6122. doi:10.1038/s41598-019-41626-y
6. Linkous AG, Yazlovitskaya EM, Hallahan DE. Cytosolic phospholipase A2 and lysophospholipids in tumor angiogenesis. *J Natl Cancer Inst*. Sep 22 2010;102(18):1398-412. doi:10.1093/jnci/djq290